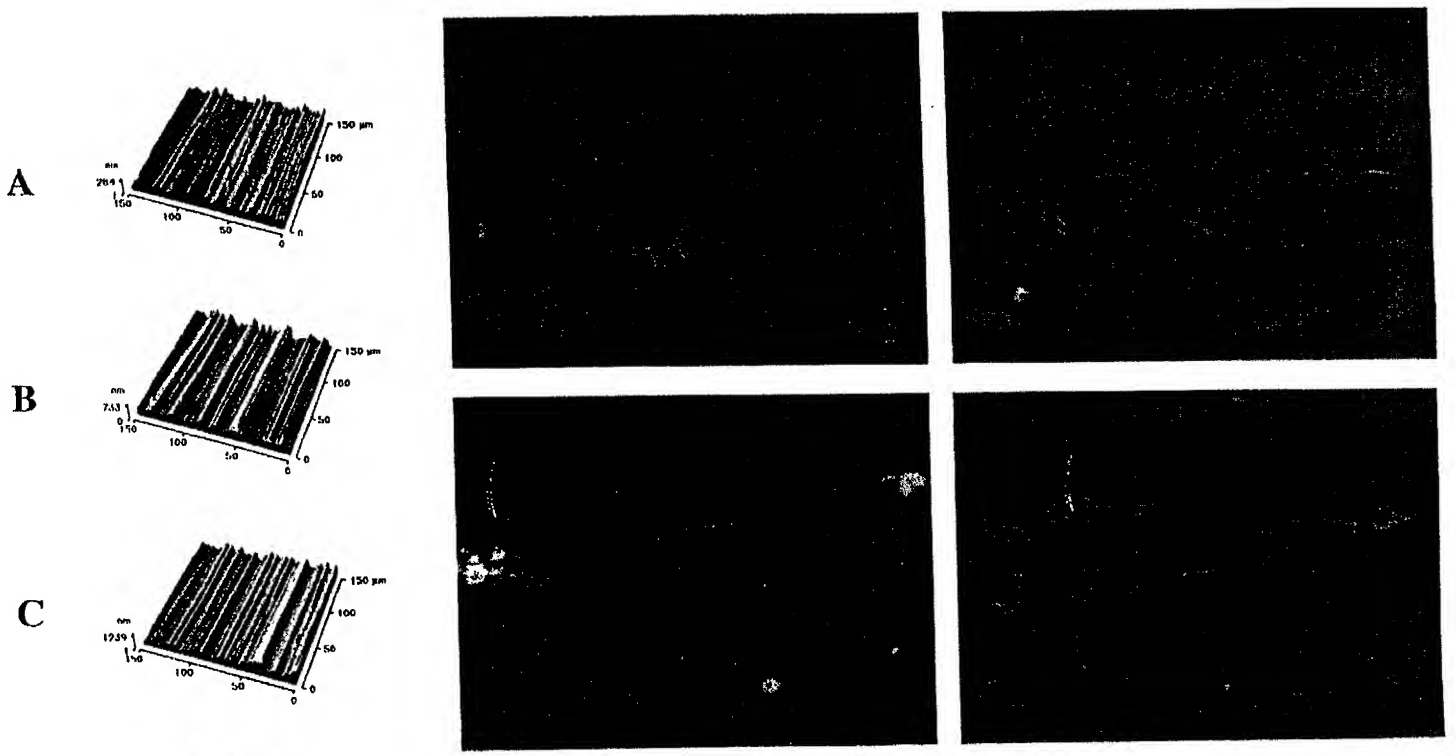

Figure 1. DRG axonal outgrowth on bed of perinatal cortical astrocytes. Astrocytes were plated on polypropylene substrates of increasing oriented groove depth (AFM profiles on the left correspond to with the same letter designation above). After reaching confluence, DRG neurons were plated on top of the astrocyte bed. Astrocytes are stained for GFAP (blue), and neurons are stained for beta-III-tubulin (red). 200X total magnification, scale bar = 100 microns.

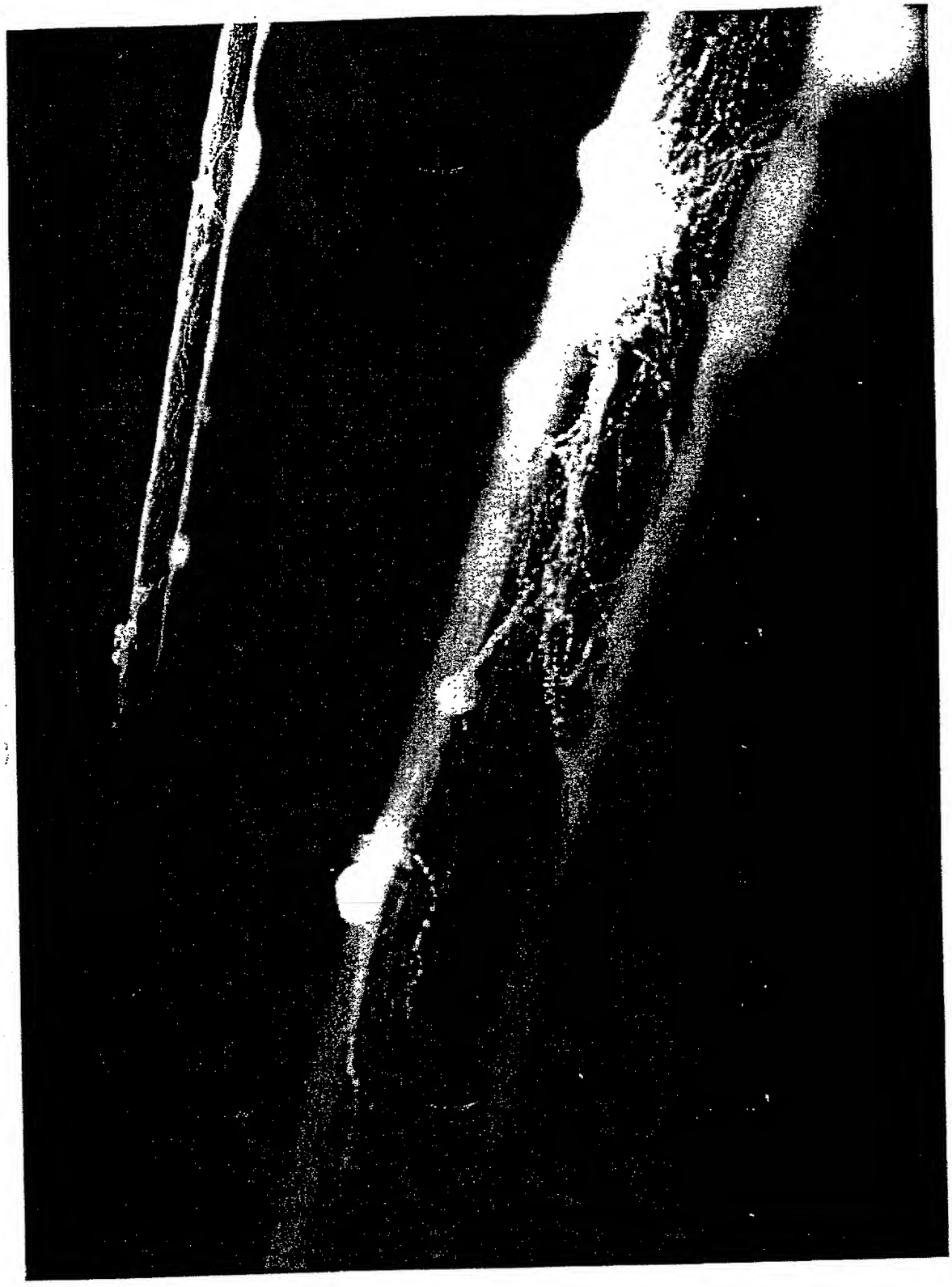

Oriented NFG Substrates: Comparison of Surface Topography

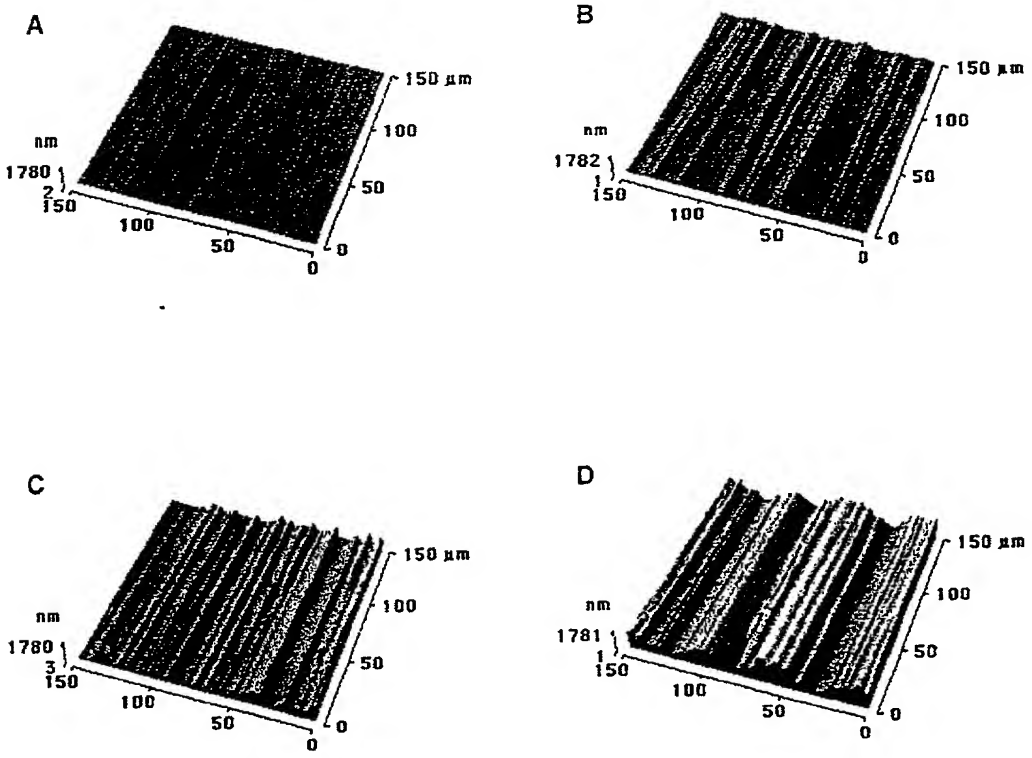

Figure 2 3

Atomic Force Microscopy Images of Oriented NFG Substrates

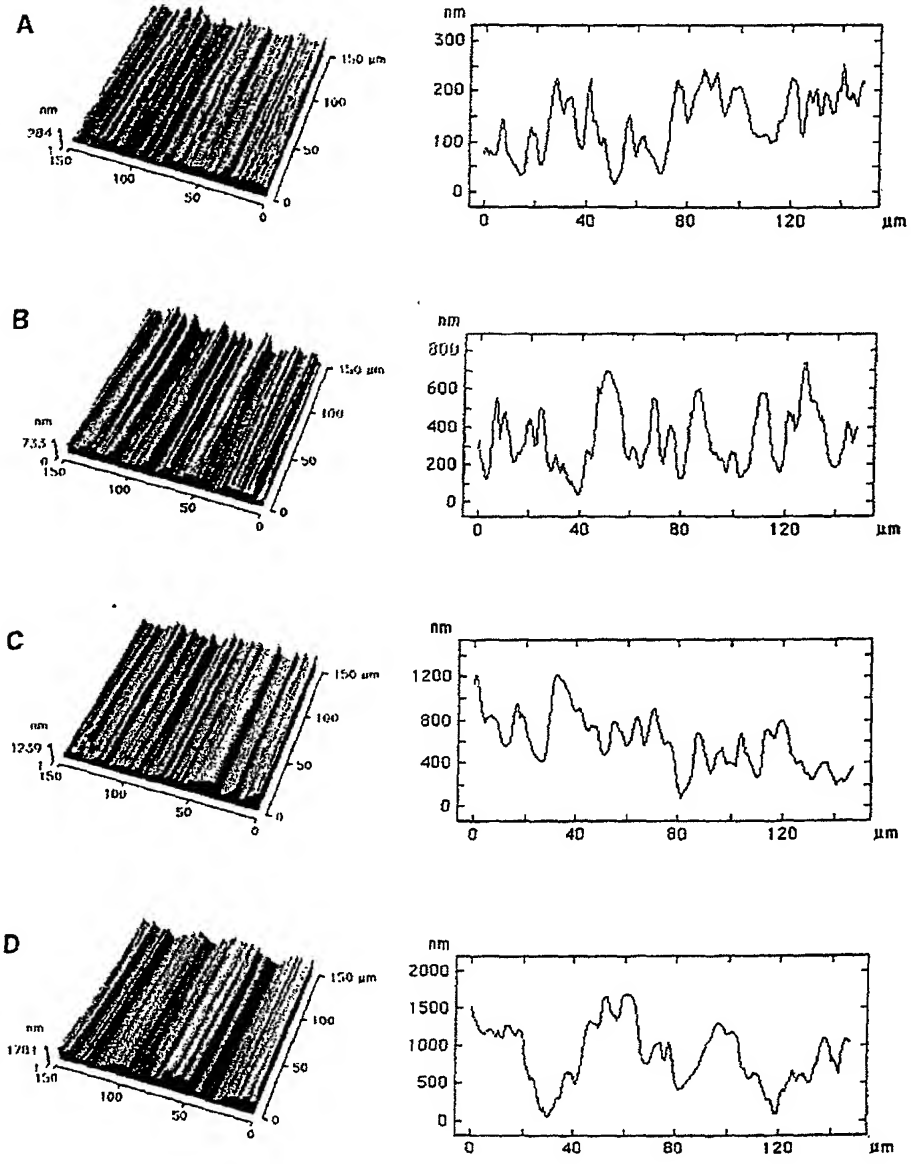

Figure 4

Meningeal Cytoskeletal Alignment on Oriented NFG Substrates

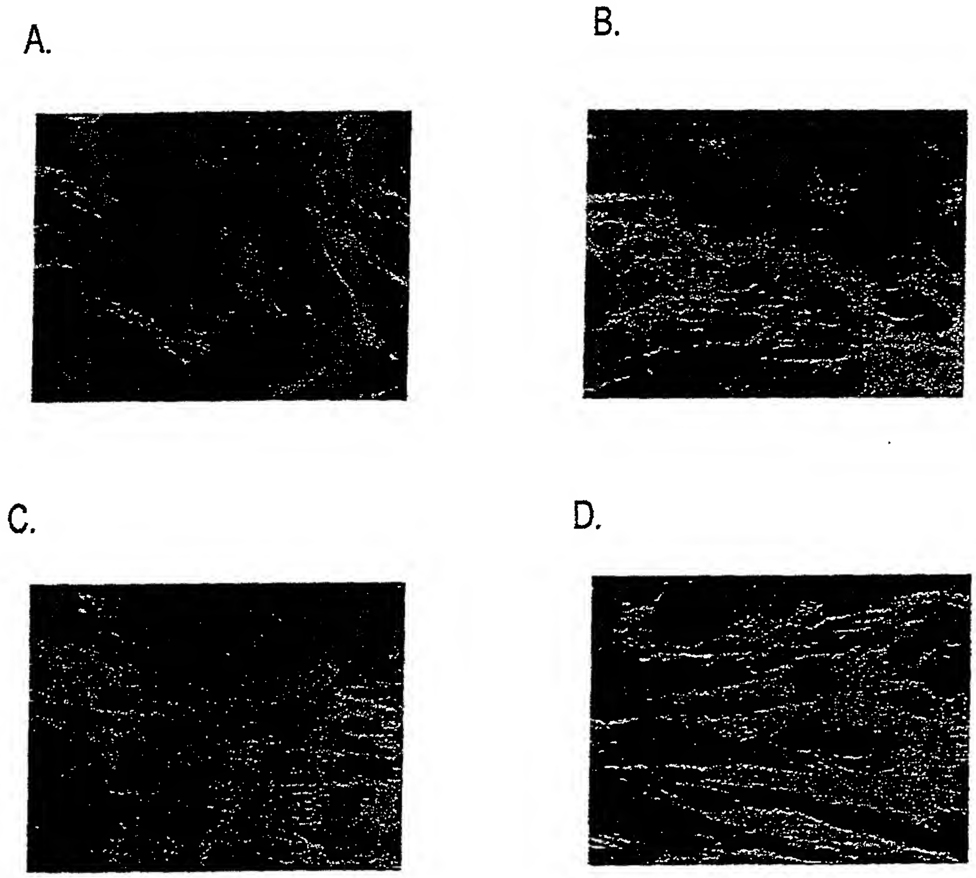

Magnification 63X.

FITC-labeled microtubules (red) and DAPI stained nuclei. Cell orientation is lost on surfaces with a surface roughness of less than 1000nm.

Figure 45

Primary Meningeal Cells on Polypropylene of Various Oriented Microtopography

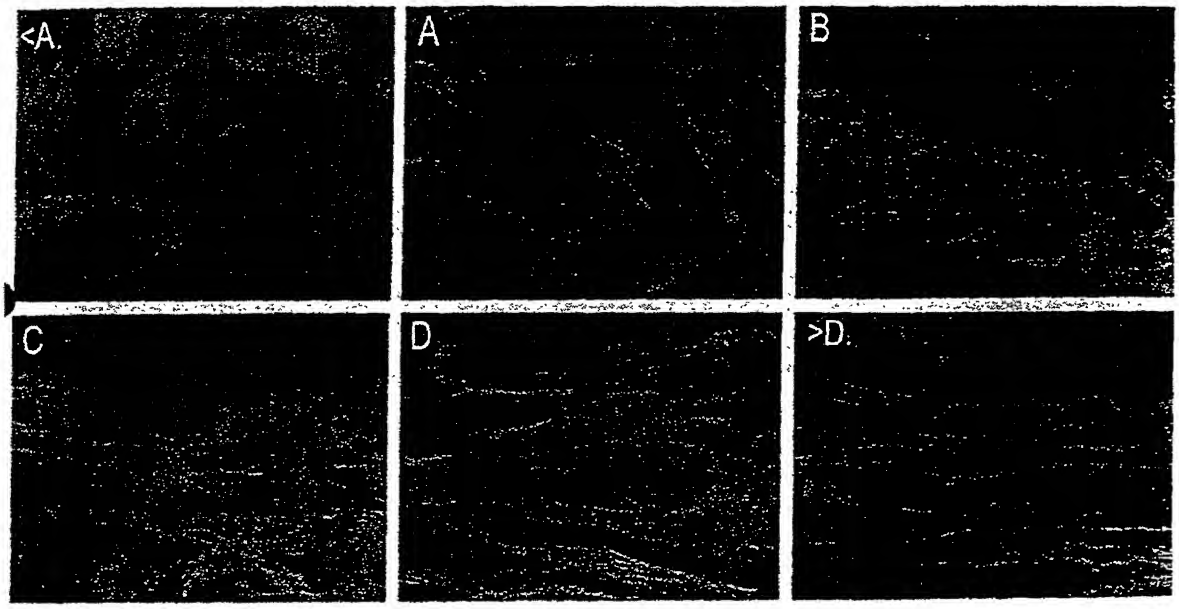

Magnification 63X

Figure 6

DRG Neurons on Polypropylene Filaments

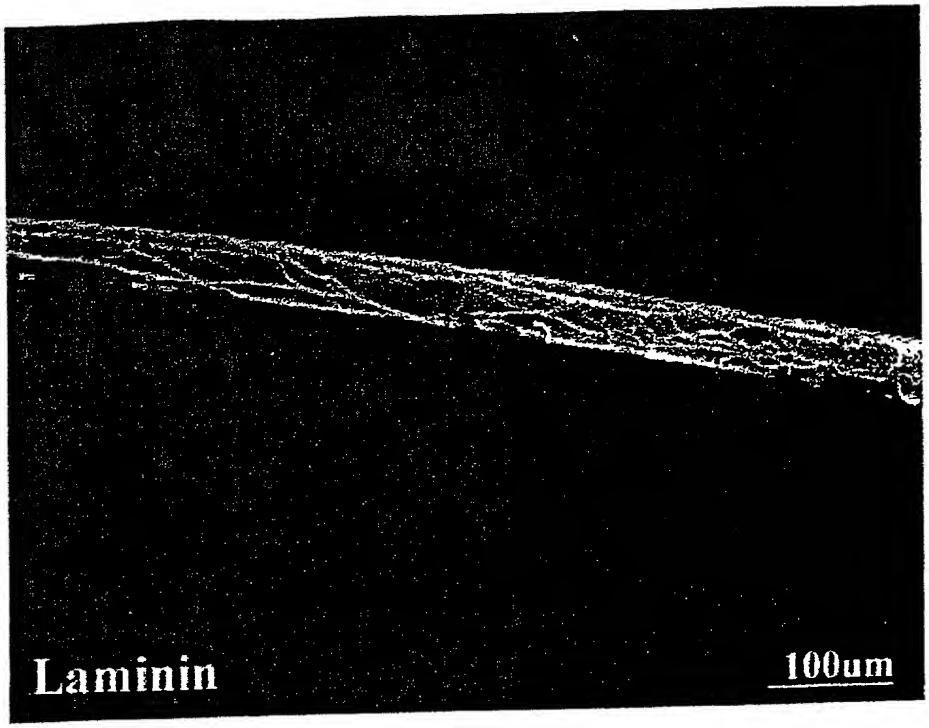

Figure 7.

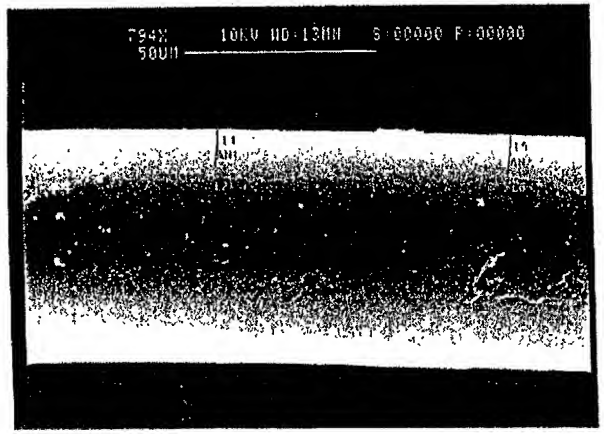

Polypropylene Fiber: 70 micron smooth

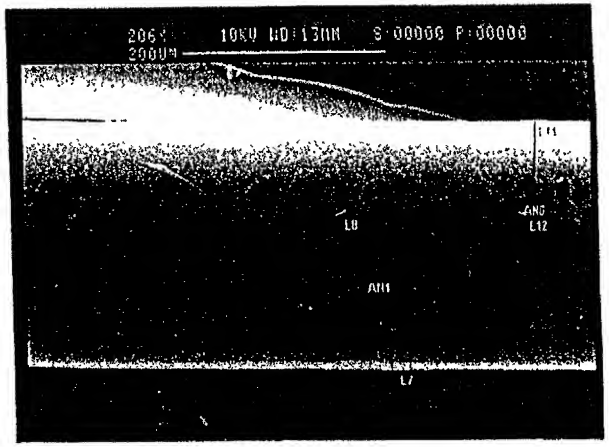

Polypropylene Fiber: 250 micron smooth

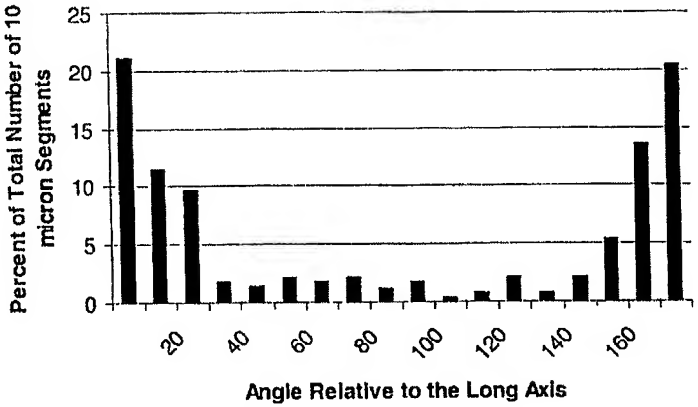

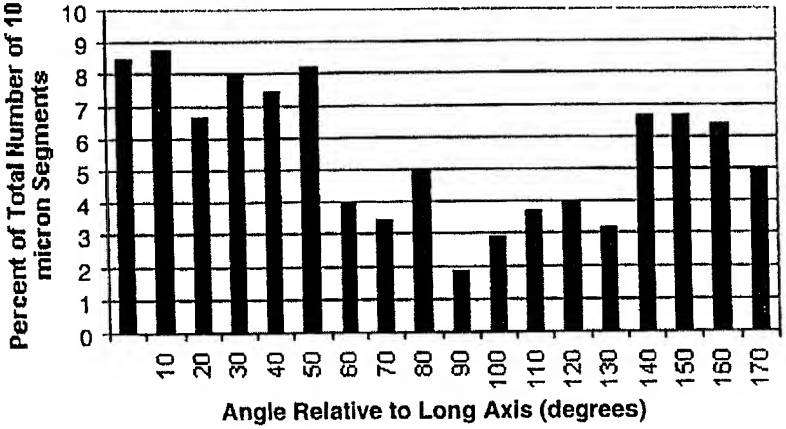

Figure 1. Comparison of the effects of filament diameter on orientation of neuronal process extension. P1 rat DRG neurons were plated on laminin-treated polypropylene filaments and allowed to grow for 24 hours prior to fixation. Sample were processed by standard methods for scanning electron microscopy. Representative images and a summary of data are shown for two filament sizes.

Astrocyte Attachment to Polypropylene: Effect of Laminin and L1-Fc

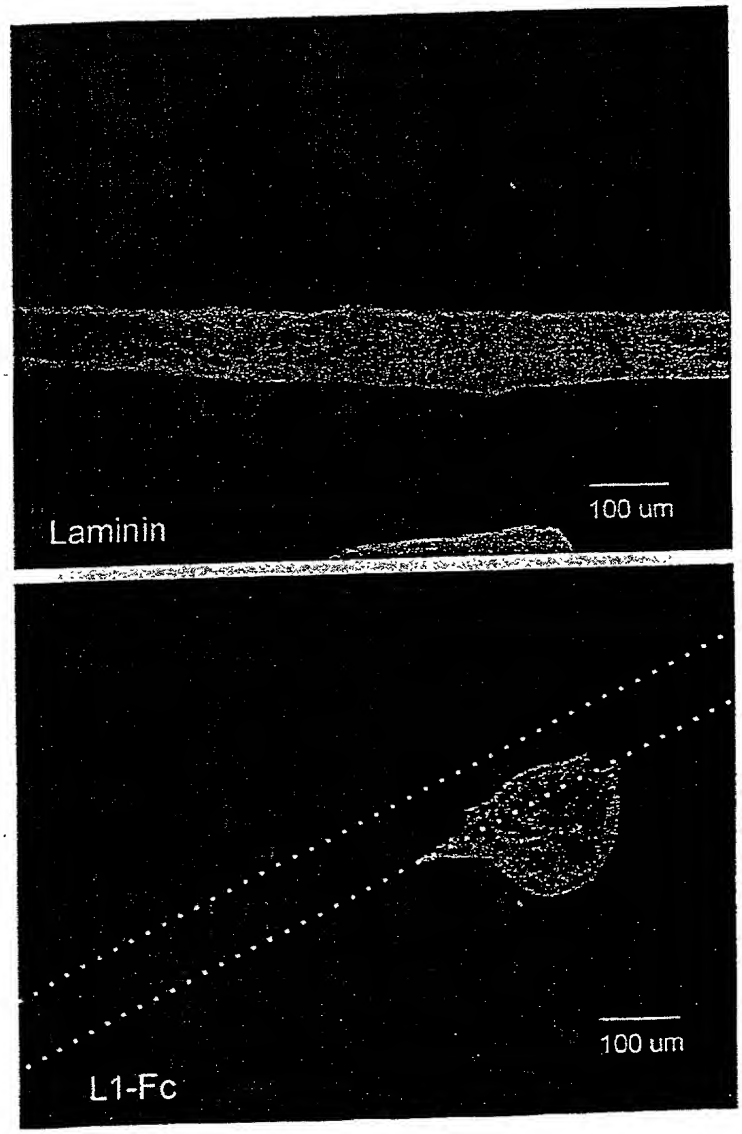

Figure 8

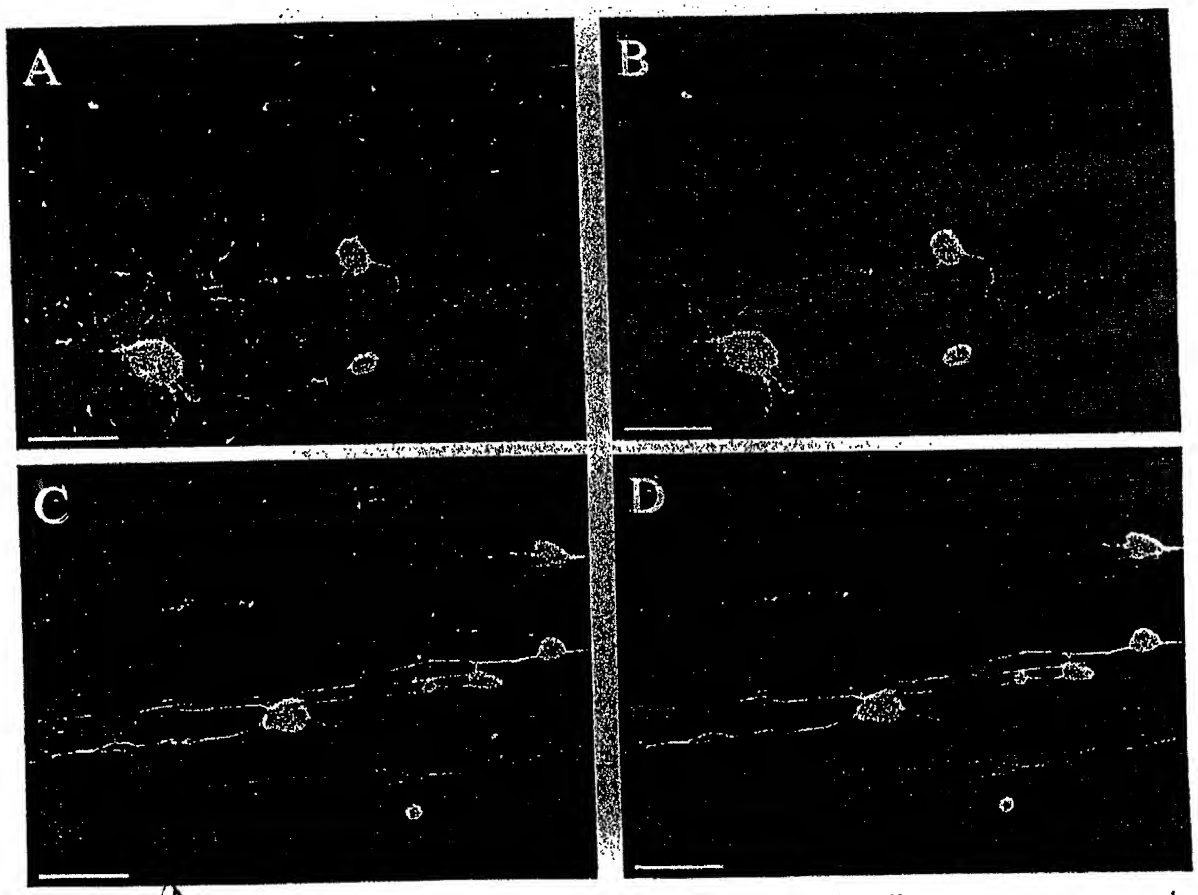

Figure 2. A comparison of neurite outgrowth on meningeal cells grown on grooved substrates. Panels A and B depict the smoothest surface, while panels C and D show a highly grooved surface. Meningeal cells are labeled with cellular fibronectin (green), neurons with beta-III-tubulin (red), and all nuclei with DAPI (blue). Panel B depicts the same field as A, and panel D depicts the same field as C. In both B and D, the green channel for fibronectin has been omitted to enhance the contrast of the beta-III-tubulin stain. Total magnification is 200X, scale bar = 100 microns.

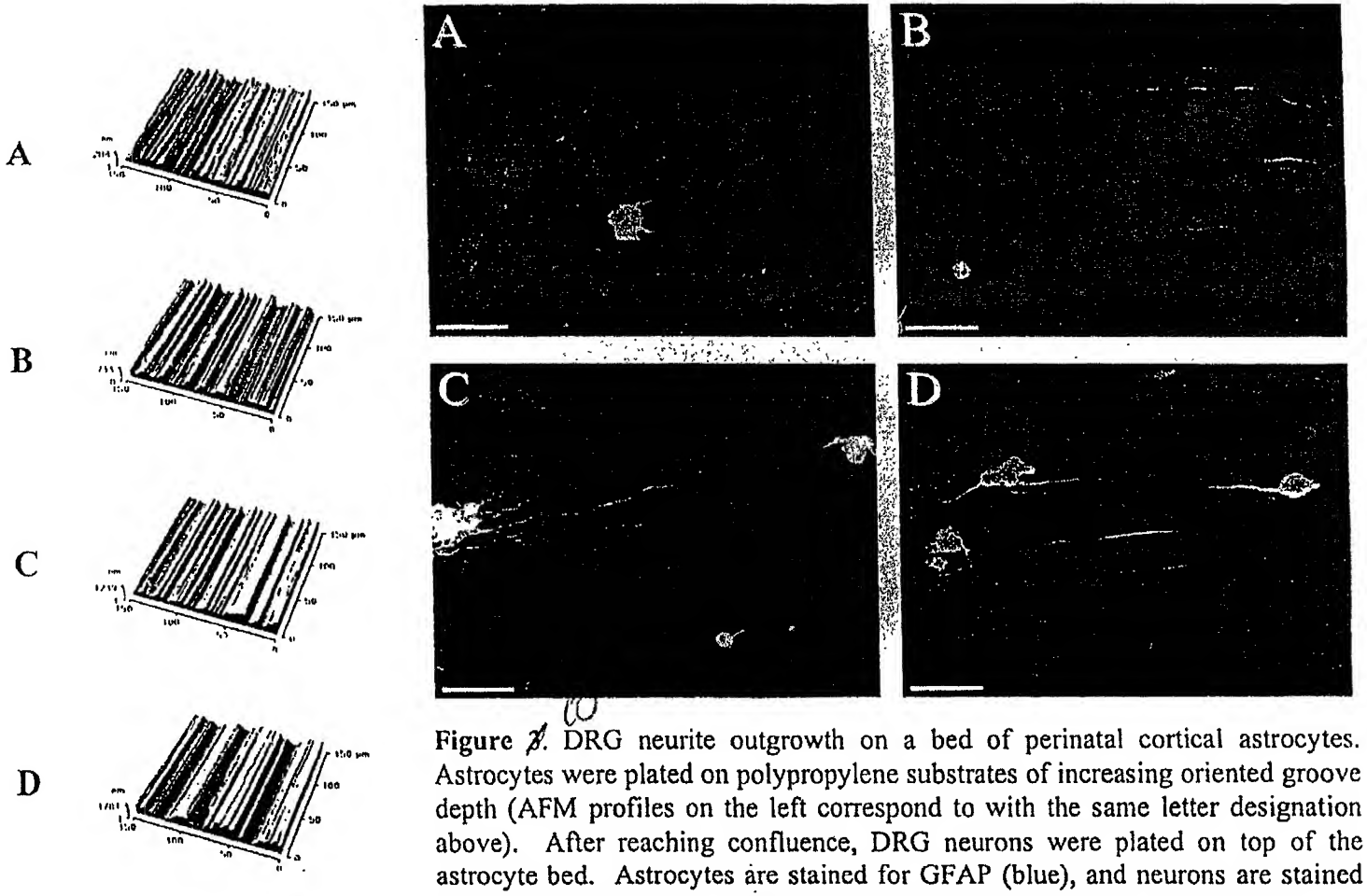

Figure 8. DRG neurite outgrowth on a bed of perinatal cortical astrocytes. Astrocytes were plated on polypropylene substrates of increasing oriented groove depth (AFM profiles on the left correspond to with the same letter designation above). After reaching confluence, DRG neurons were plated on top of the astrocyte bed. Astrocytes are stained for GFAP (blue), and neurons are stained for beta-III-tubulin (red). 200X total magnification, scale bar = 100 microns.

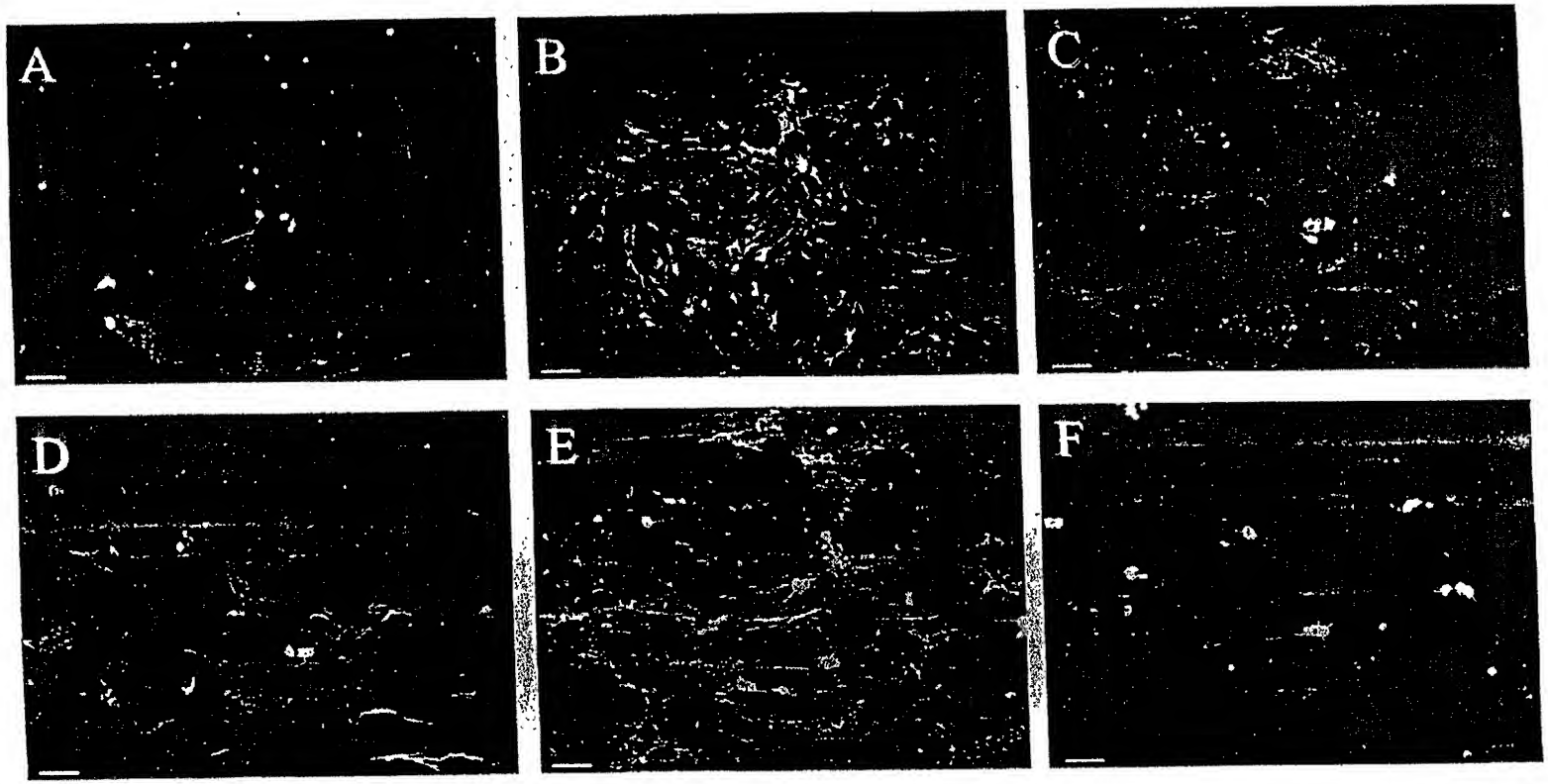

Figure 4. DRG outgrowth on a bed of perinatal cortical astrocytes. Astrocytes were plated on polypropylene substrates of increasing groove depth. The underlying astrocytes were stained for actin (red). Neurons were stained for beta-III-tubulin (green). Oriented groove depth increases from panel A through F (A=smoothest and F=roughest). 100X total magnification, scale bar = 100 microns. A higher power of view of the same conditions is shown on the next figure.

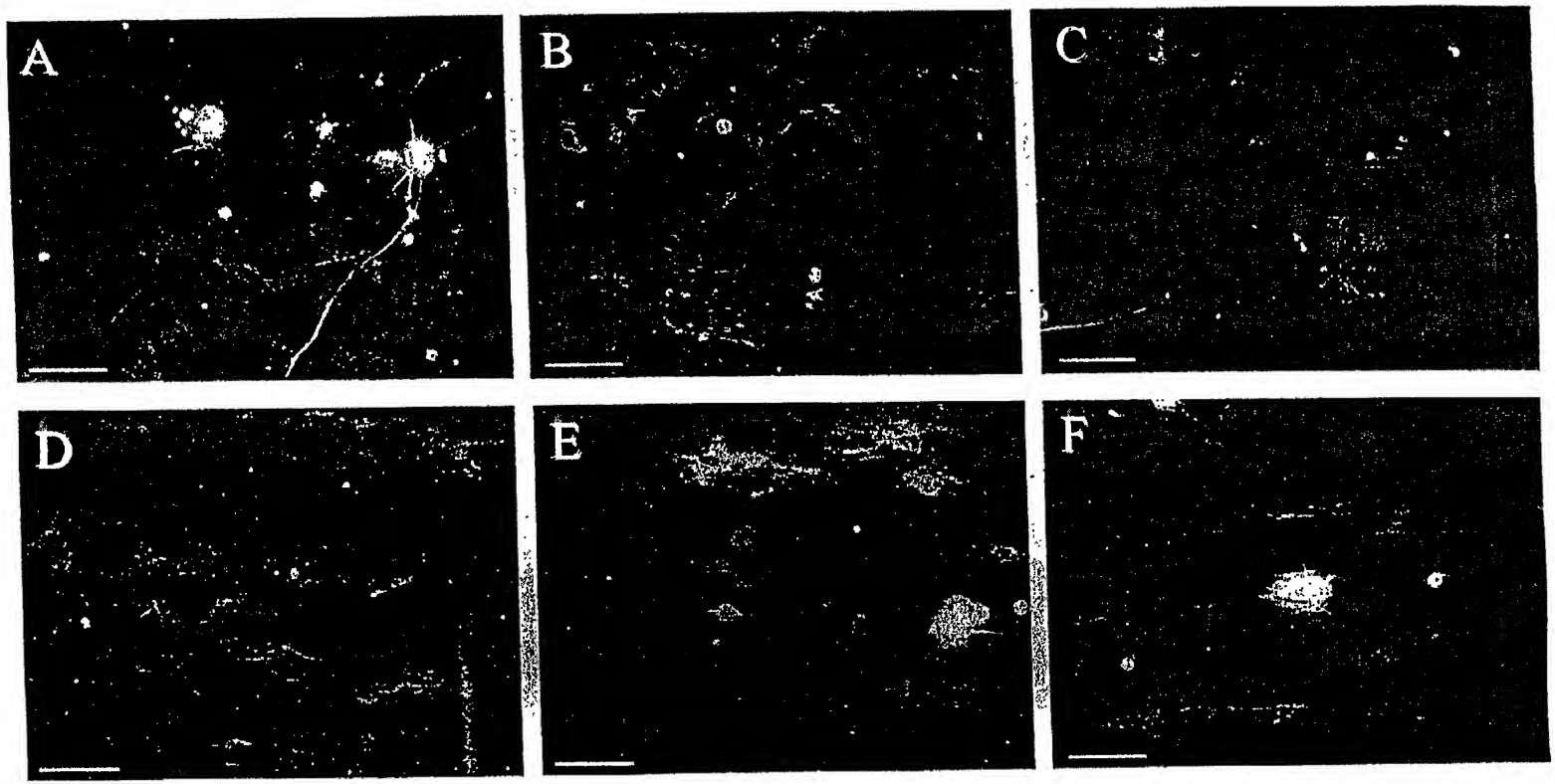

Figure 8. DRG outgrowth on a bed of perinatal cortical astrocytes. Astrocytes were plated on polypropylene substrates of increasing groove depth. The underlying astrocytes were stained for actin (red). Neurons were stained for beta-III-tubulin (green). Oriented groove depth increases from panel A through F (refer to corresponding AFM images of substrates). 200X total magnification, scale bar = 100 microns.

FIGURES:

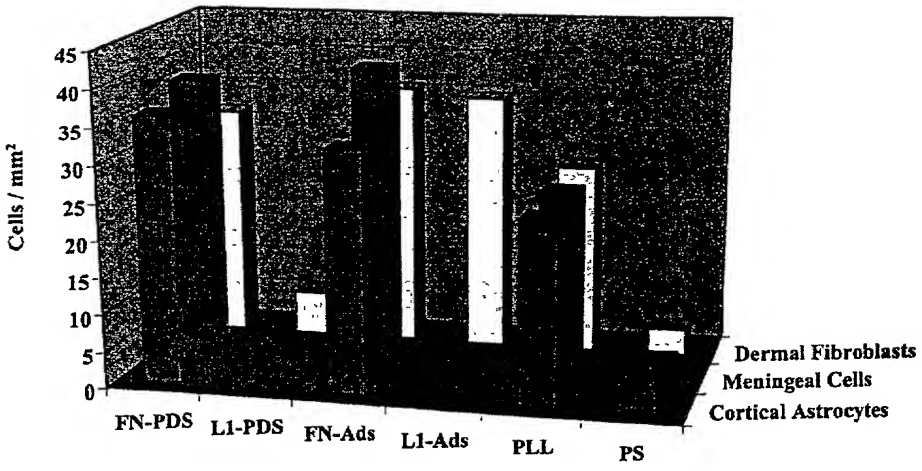

Figure 13. Comparison of cell attachment to substrates treated with fibronection, L1, and poly-l-lysine. The following surface treatments were compared: fibronectin covalently bound to polyethylene oxide (PEO) (FN-PDS); L1 covalently bound to polyethylene oxide (PEO) (L1-PDS); fibronectin adsorbed to the substrate (FN-ADs); L1 adsorbed to the substrate (L1-ADs); poly-l-lysine adsorbed to the substrate (PLL); and nothing adsorbed to the substrate (PS). All cultures were maintained in the presence of serum containing media.

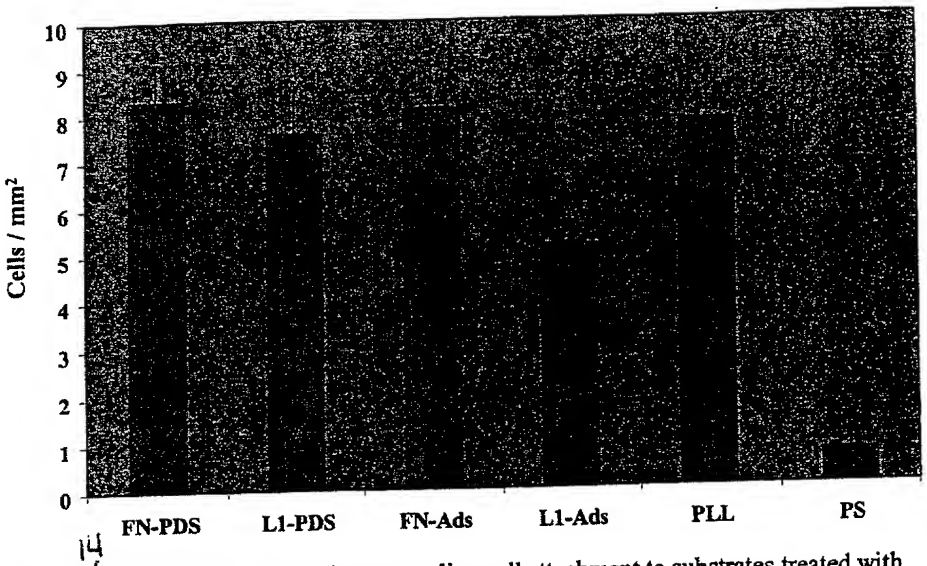

Figure 14 Comparison of dorsal root ganglion cell attachment to substrates treated with fibronection, L1, and poly-l-lysine. The following surface treatments were compared: fibronectin covalently bound to polyethylene oxide (PEO) (FN-PDS); L1 covalently bound to polyethylene oxide (PEO) (L1-PDS); fibronectin adsorbed to the substrate (FN-ADs); L1 adsorbed to the substrate (L1-ADs); poly-l-lysine adsorbed to the substrate (PLL); and nothing adsorbed to the substrate (PS). All cultures were maintained in the presence of serum containing media. Attachment to L1-Ads and PS were significantly less than other groups.

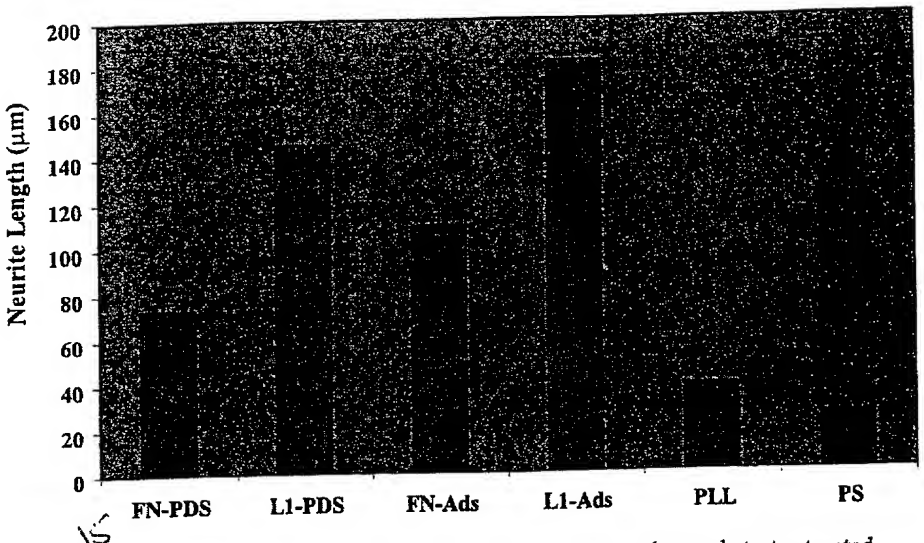

Figure 3. Comparison of dorsal root ganglion neurite outgrowth to substrates treated with fibronection, L1, and poly-l-lysine. The following surface treatments were compared: fibronectin covalently bound to polyethylene oxide (PEO) (FN-PDS); L1 covalently bound to polyethylene oxide (PEO) (L1-PDS); fibronectin adsorbed to the substrate (FN-ADs); L1 adsorbed to the substrate (L1-ADs); poly-l-lysine adsorbed to the substrate (PLL); and nothing adsorbed to the substrate (PS). All cultures were maintained in the presence of serum containing media. Outgrowth on both L1 treatments were significantly greater that FN treatments which were also greater that PLL and PS groups.

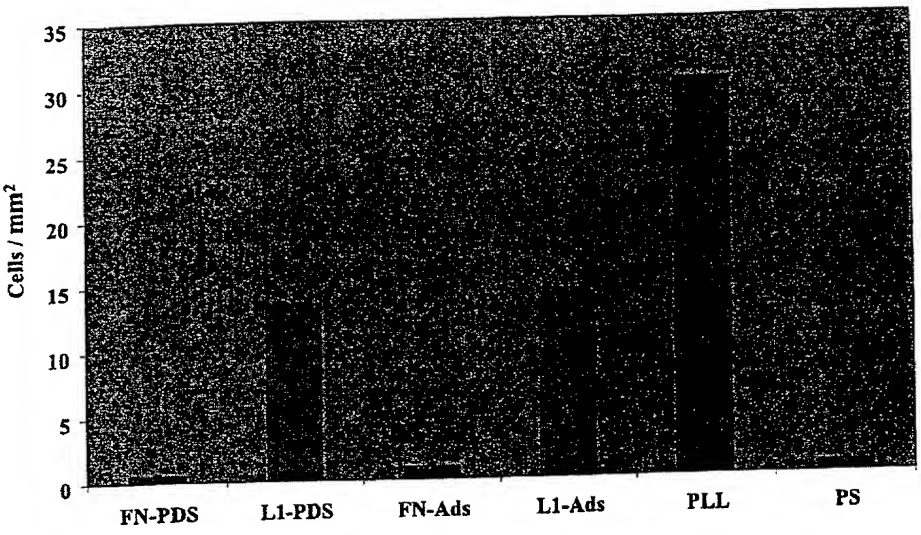

Figure 4. Comparison of cerebellar granule neuron cell attachment to substrates treated with fibronection, L1, and poly-l-lysine. The following surface treatments were compared: fibronectin covalently bound to polyethylene oxide (PEO) (FN-PDS); L1 covalently bound to polyethylene oxide (PEO) (L1-PDS); fibronectin adsorbed to the substrate (FN-ADs); L1 adsorbed to the substrate (L1-ADs); poly-l-lysine adsorbed to the substrate (PLL); and nothing adsorbed to the substrate (PS). All cultures were maintained in the presence of serum containing media. Attachment to L1-treatments and PLL were significantly greater than other groups.

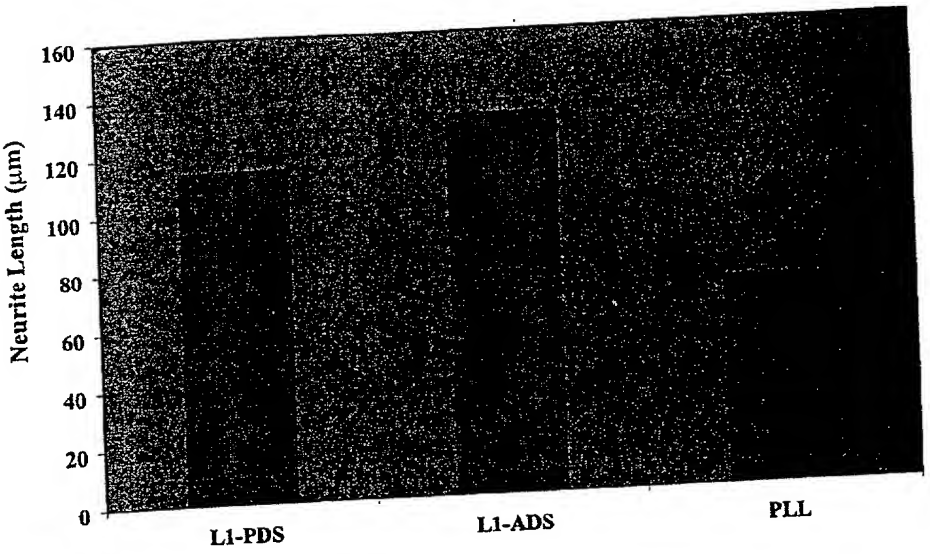

17

Figure 5. Comparison of cerebellar granule neuron neurite outgrowth on substrates treated with L1 and poly-l-lysine. The following surface treatments were compared: fibronectin covalently bound to polyethylene oxide (PEO) (FN-PDS); L1 covalently bound to polyethylene oxide (PEO) (L1-PDS); fibronectin adsorbed to the substrate (FN-ADs); L1 adsorbed to the substrate (L1-ADs); poly-l-lysine adsorbed to the substrate (PLL); and nothing adsorbed to the substrate (PS). All cultures were maintained in the presence of serum containing media. No outgrowth occurred on the FN or the PS conditions (data not shown). Outgrowth on both L1 treatments were significantly greater PLL.

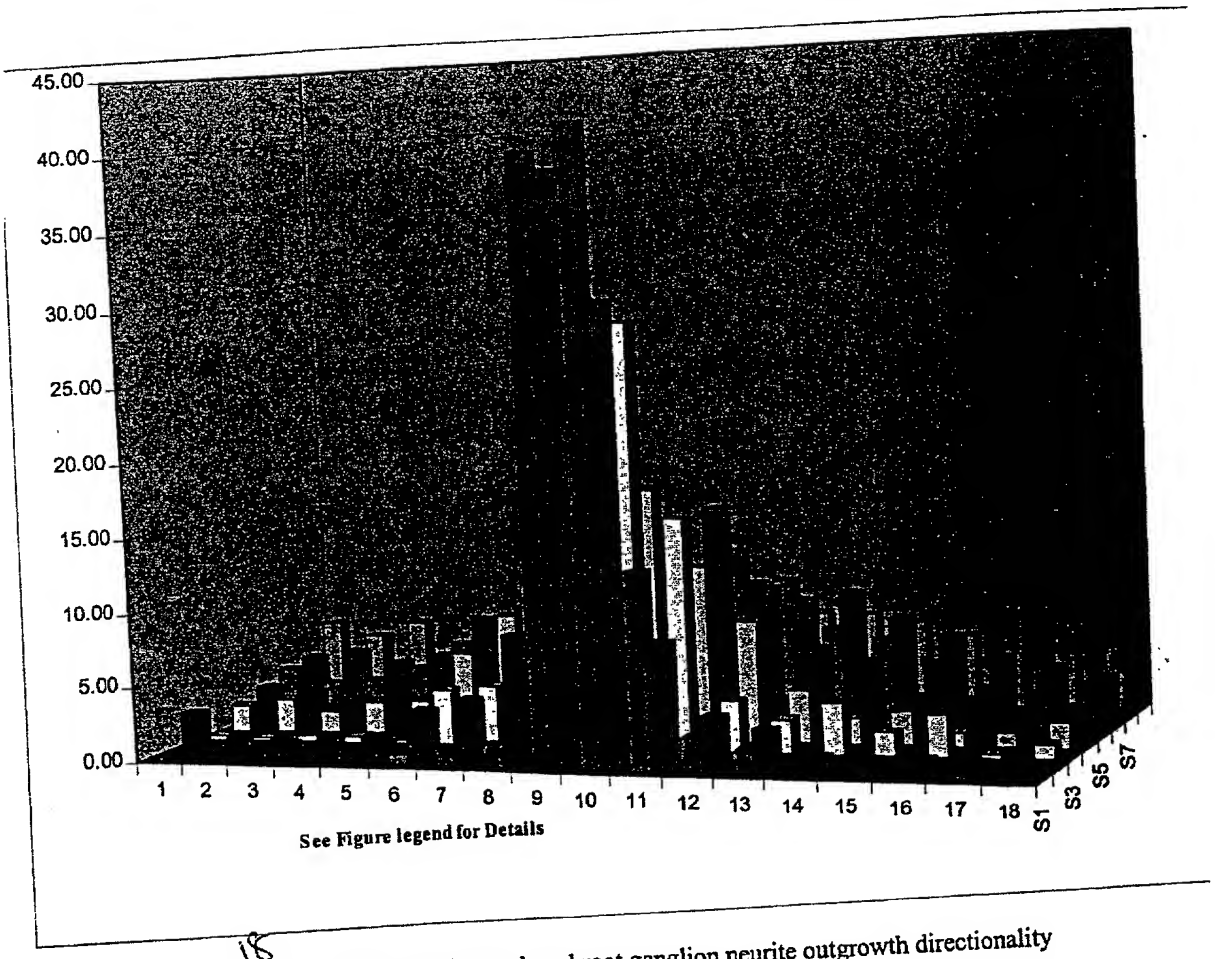

18

Figure 6. Comparison of primary dorsal root ganglion neurite outgrowth directionality on polypropylene substrates with differing radius of curvature. The following surfaces were diameters (microns): S1 was 53; S2 was 95; S3 was 200; S4 was 300; S5 was 500; and S6 was a flat surface. Data is reported as the percentage of outgrowth in angles segment of 10 degrees where 1=0; 2=10; 3=20;...10=90 or growth perpendicular to the long axis; and so on. On-going studies will fill in the data by examining smaller diameter filaments and by increasing the number of observations at each filament diameter so that a model can be created that predicts cell behavior as a function of filament a diameter.

Figure 7. Conceptual Schematic

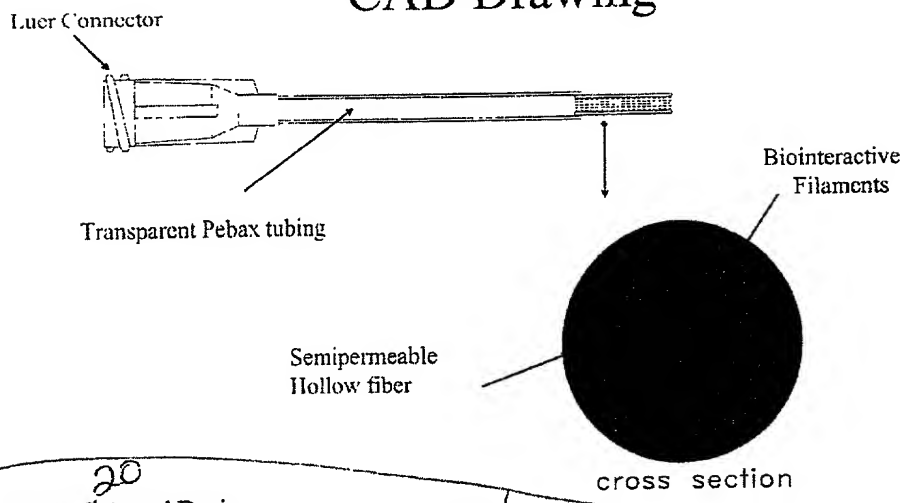

Figure 8 Actual Device

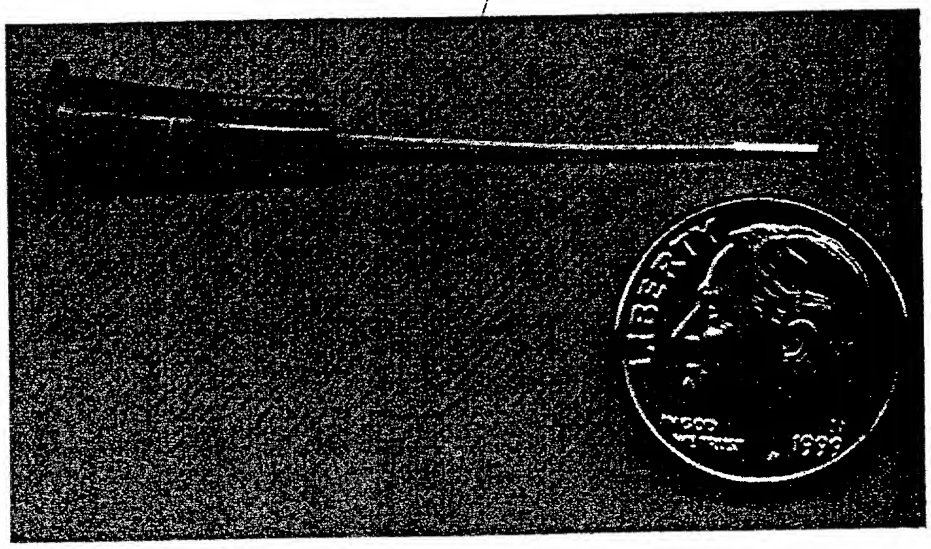

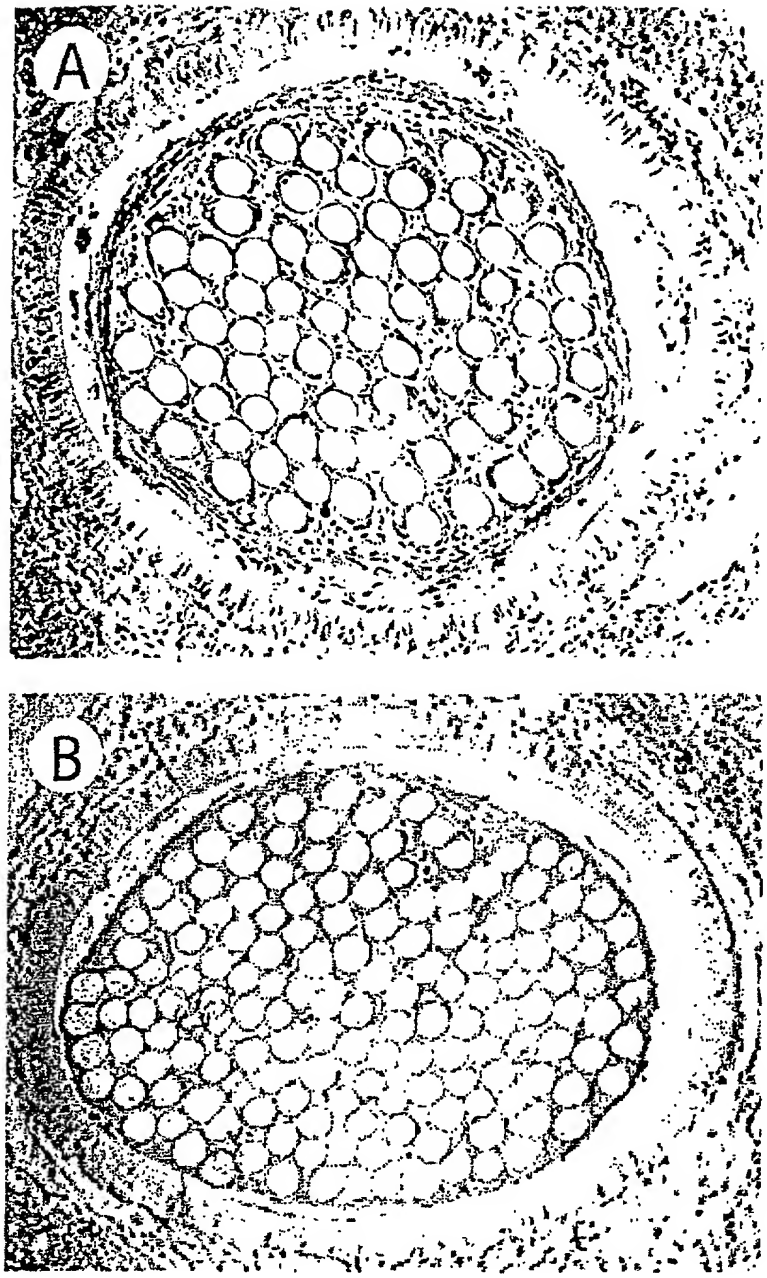

Figure ~~11~~ 21

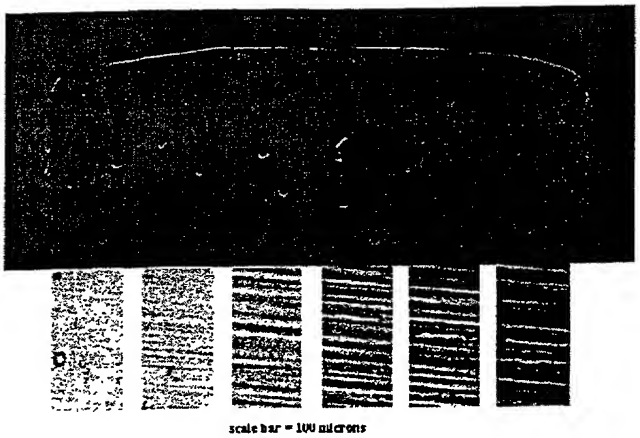

Figure 22 Low power light micrograph of polymeric substrate, with varying degrees of microtexture, used for cell culture studies.

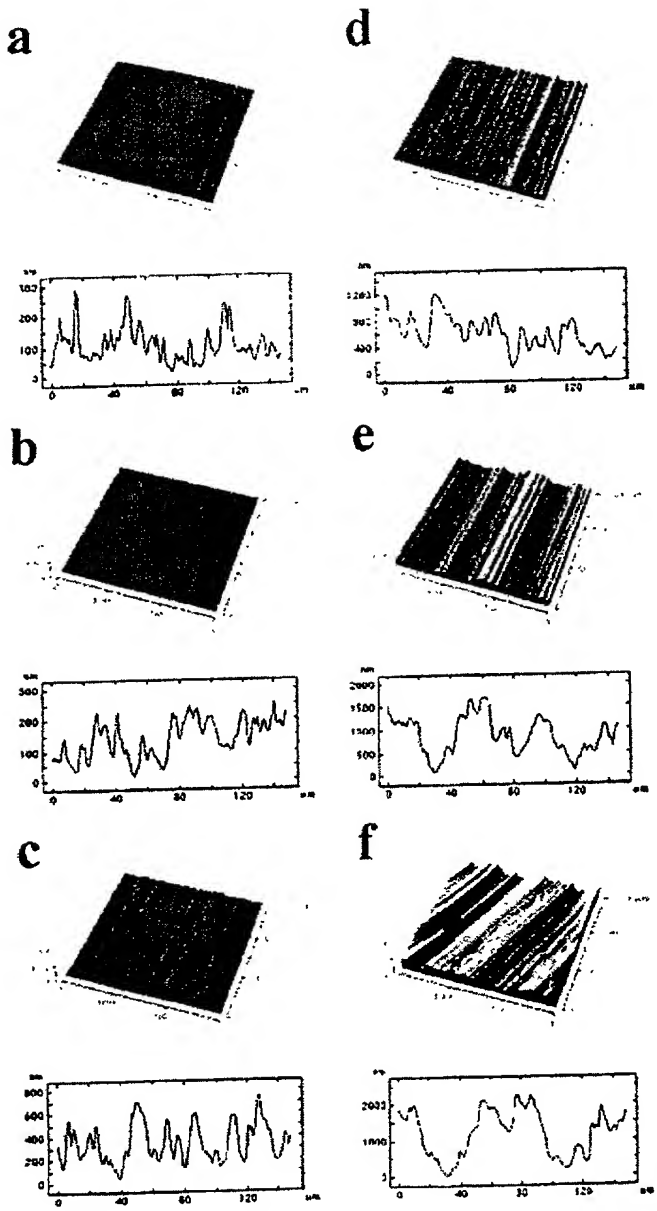

Figure 9 Representative images of varying surface topography of substrate shown in figure 8 as determined by scanning atomic force microscopy.

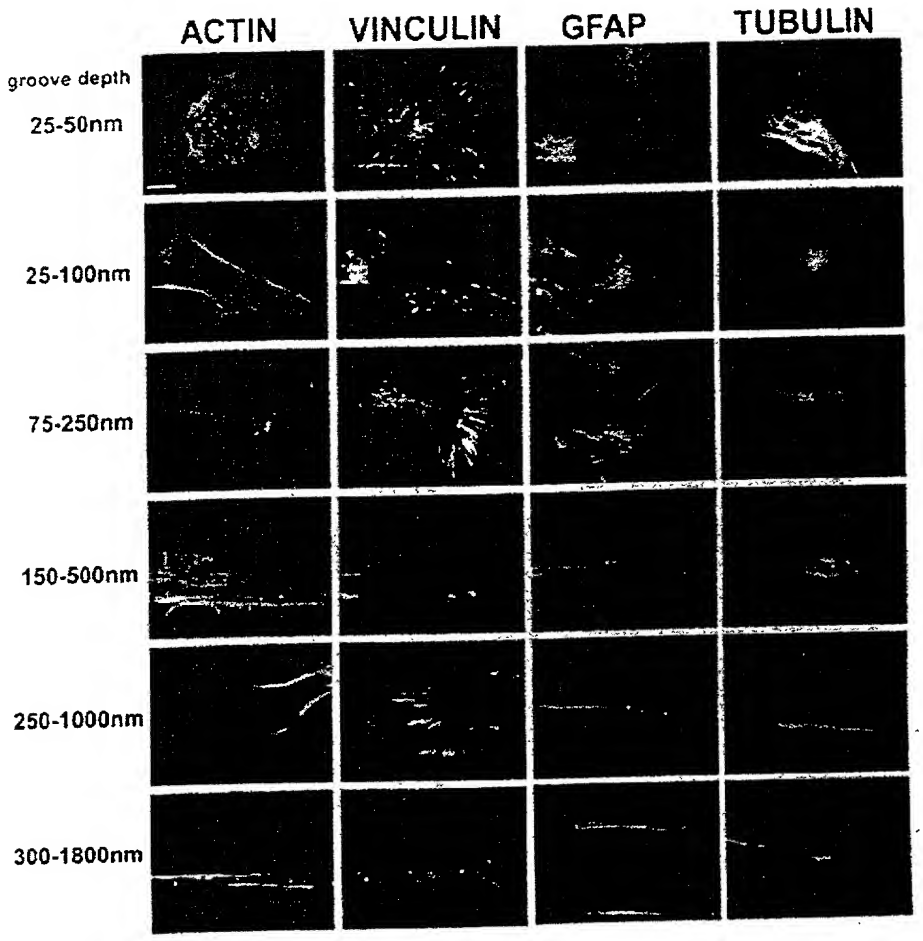

Figure 10 Gradual alignment of the astrocyte cytoskeleton as a function of increasing groove depth in the surface topography. 100x immunofluorescence photomicrographs of cells stained for a range of cytoskeletal proteins. Scale bar = 20 microns.

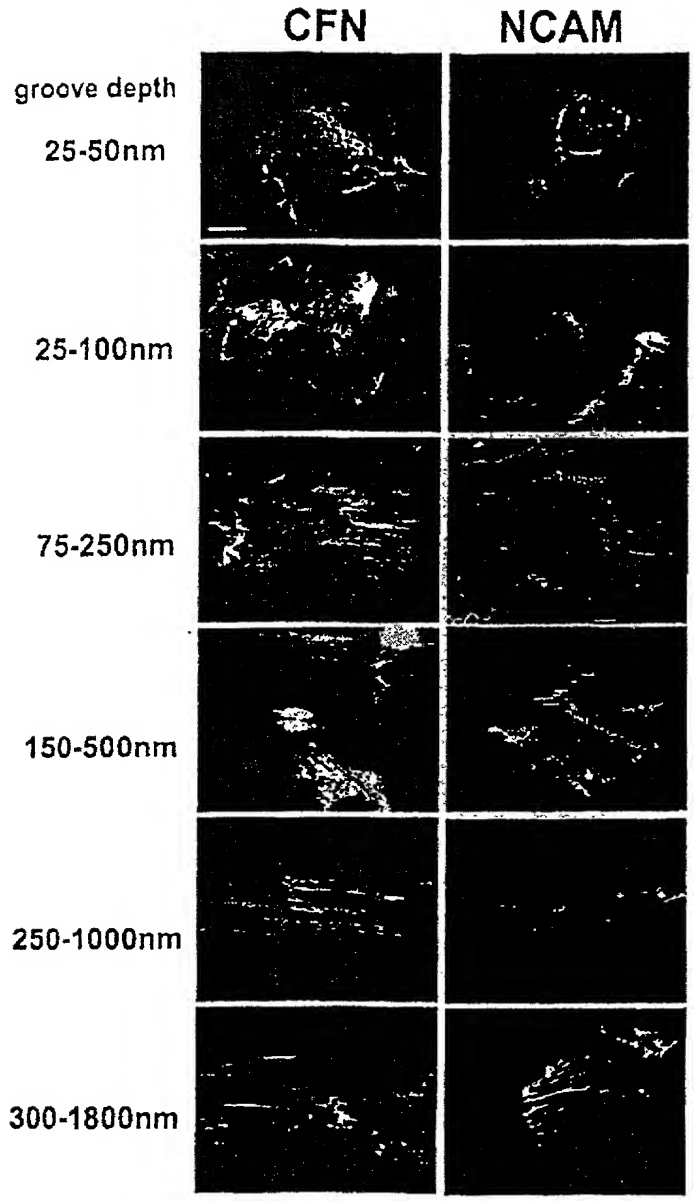

Figure 25 Gradual alignment of astrocyte-derived extracellular matrix and cell adhesion proteins as a function of increasing groove depth. 100x immunofluoresescence photomicrographs of cells stained for CFN or NCAM.

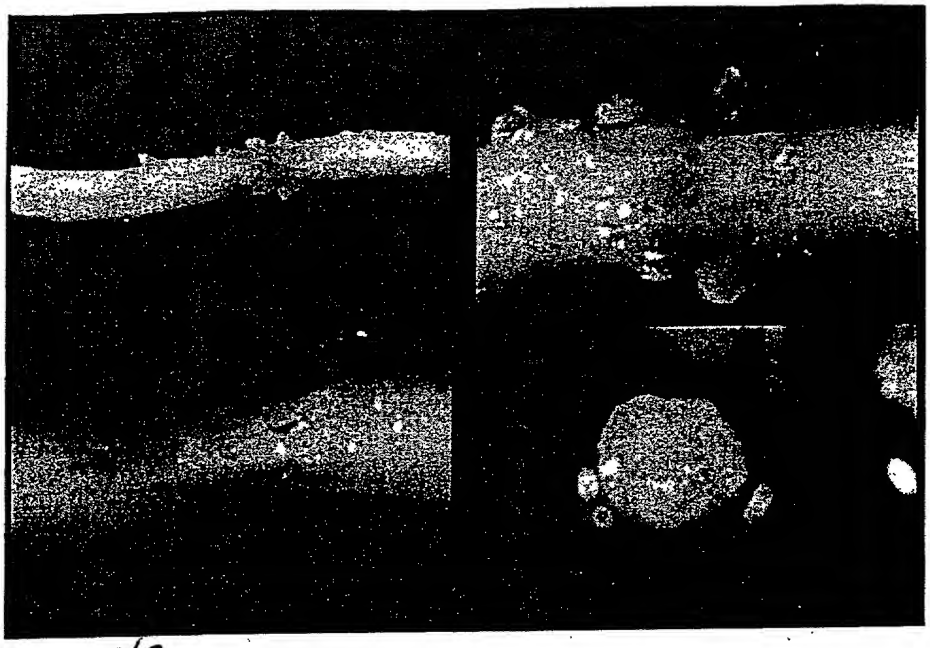

Figure 12 Photographs of rat thoracic spinal cord with dorsal hemisection and implantation of a multi-filament device. The integration of the device is shown from dorsal view before (above) and after (bottom left) removal of the dura. The presence of the device within the dorsal lesion space can be seen in transverse section in the bottom right.

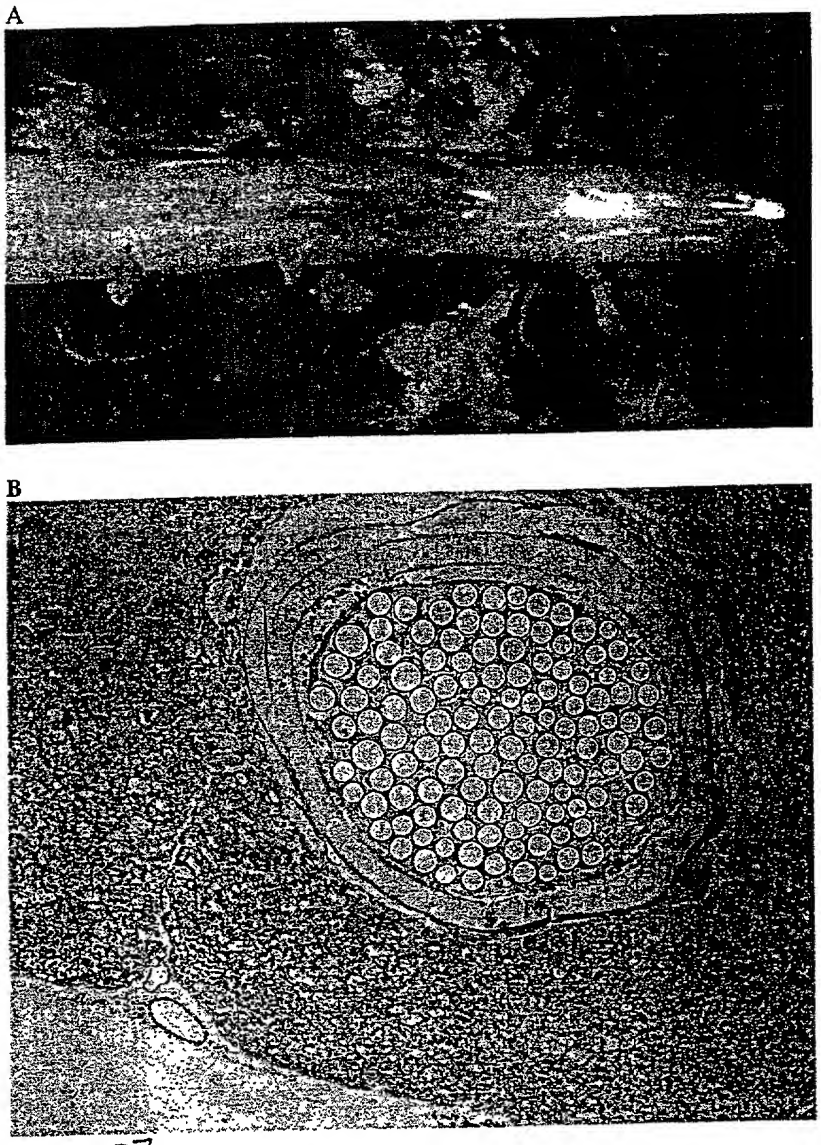

Figure 13 A) Dorsal view of the spinal cord following fixation for histology and exposure within the vertebral canal. The site of injury and implantation of the multi-filament device is clearly visible, though the reaction to the implant is minimal.
B) Transverse section through the multifilament device within the spinal cord, just outside the injury zone. The filaments within the semi-permeable tube are clearly visible, surrounded by cellular material that has completely invaded the lumenal space of the device. Luxol fast blue/H & E stain.

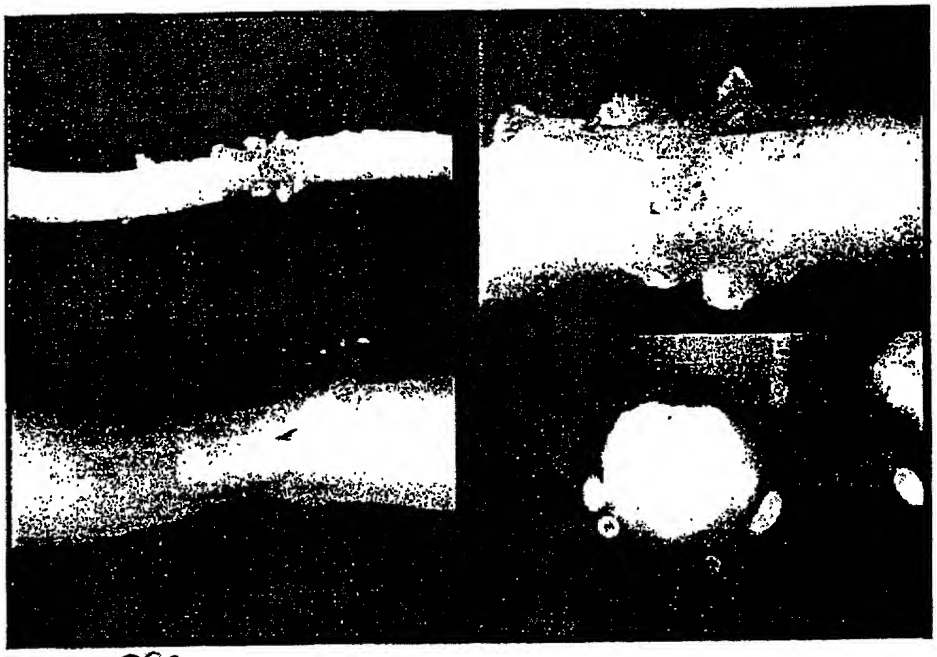

Figure ~~12~~ 28 Photographs of rat thoracic spinal cord with dorsal hemisection and implantation of a multi-filament device. The integration of the device is shown from dorsal view before (above) and after (bottom left) removal of the dura. The presence of the device within the dorsal lesion space can be seen in transverse section in the bottom right.

P1 DRG Neurons onSubstrate Immobilized Chemically-modified Laminin

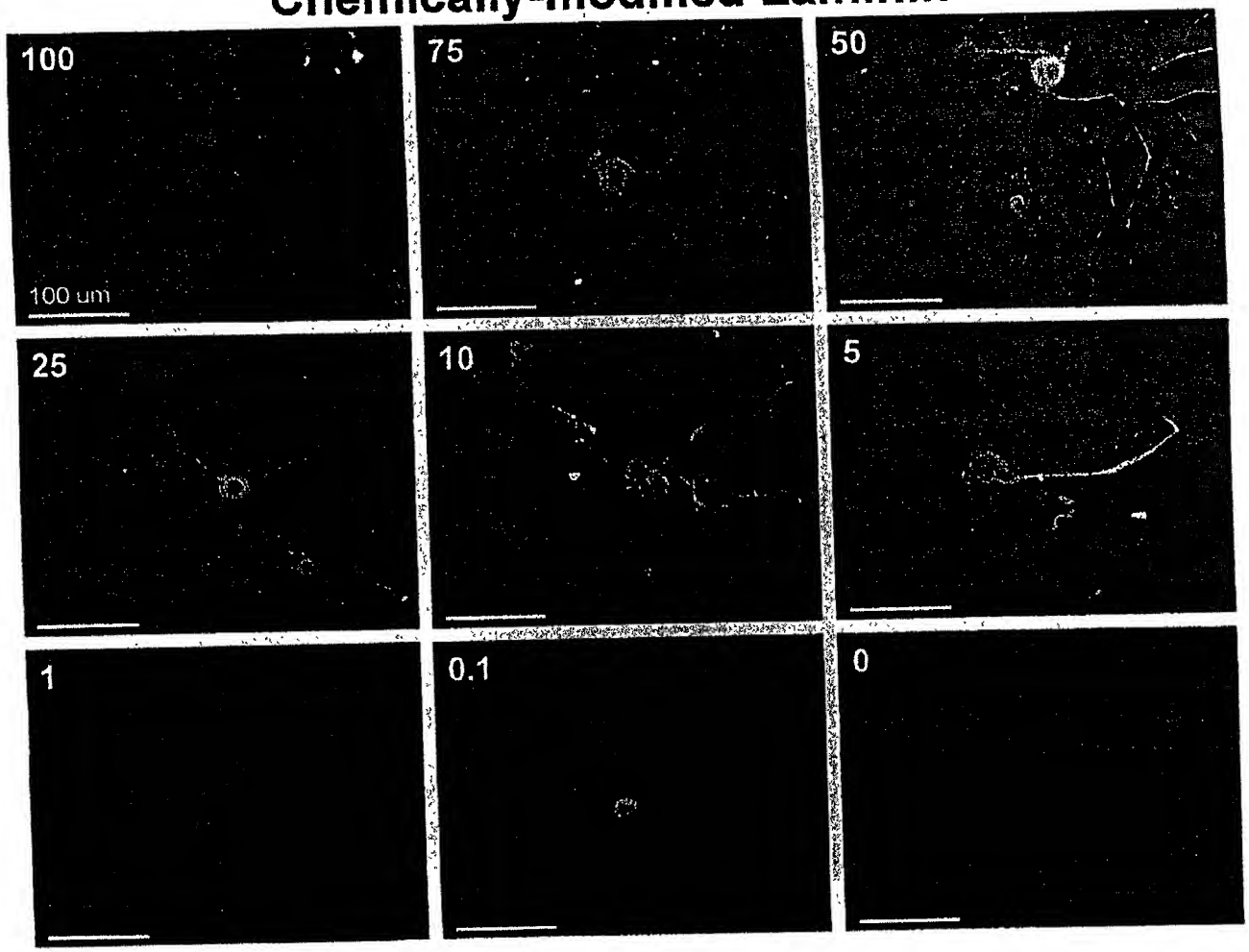

Figure 29

P1 DRG Neurons on Substrate Immobilized Chemically-modified Fibronectin

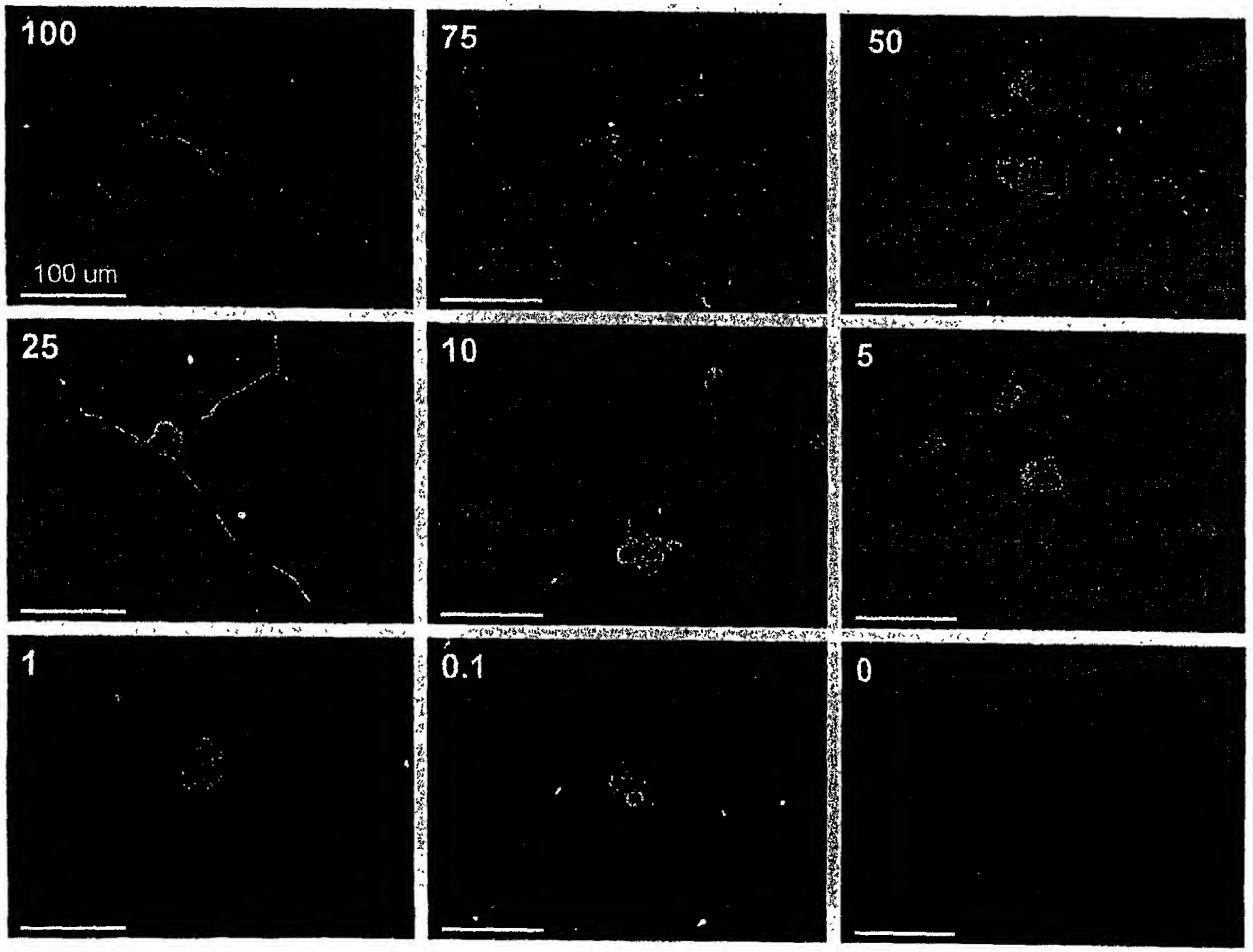

Figure 30